Effect of Pressure on the Tertiary Structure and Dynamics of Folded Basic Pancreatic Trypsin Inhibitor

Hua Li, Hiroaki Yamada,[#] and Kazuyuki Akasaka
*Department of Molecular Science, Graduate School of Science and Technology, and [#]Department of Chemistry, Faculty of Science, Kobe University, Kobe 657-8501, Japan

ABSTRACT The on-line high-pressure cell NMR technique was used to study pressure-induced changes in the tertiary structure and dynamics of a globular protein, basic pancreatic trypsin inhibitor (BPTI). Practically all the proton signals of BPTI were observed with ^{1}H two-dimensional NMR spectroscopy at 750 MHz at variable pressure between 1 and 2000 bar. Chemical shifts, nuclear Overhauser effect (NOE), and line shapes were used to analyze conformational and dynamic changes of the protein as functions of pressure. Linear, reversible, but nonuniform pressure-induced chemical shift changes of practically all the C^α protons and side chain protons showed that the entire secondary and tertiary structures are altered by pressure within the folded ensemble of BPTI. The high field shift tendency of most side chain proton signals and the increase in NOE intensities of some specific side chain protons indicated a site-specific compaction of the tertiary structure. Pressure dependence of ring flip rates was deduced from resonance line shapes of the slices of the two-dimensional NMR spectrum for ring proton signals of Tyr-35 and Phe-45. The rates of the flip-flop motions were considerably reduced at high pressure, from which activation volumes were determined to be 85 ± 20 Å^3 (or 51.2 ml/mol) and 46 ± 9 Å^3 (or 27.7 ml/mol) for Tyr-35 and Phe-45, respectively, at 57°C. The present experiments confirm that pressure affects the entire secondary and tertiary structures of a globular protein with specific compaction of a core, leading to quite significant changes in slow internal dynamics of a globular protein.

INTRODUCTION

Characterization of the dynamic feature of proteins in solution remains an area of intense interest due to implicated relationships between protein dynamics and the structure and function of proteins. The application of hydrostatic pressure to a protein in an aqueous solution is an active field for extracting the nature of protein dynamics and stability. Investigation of pressure effects on the protein structure delineates its volumetric features (Chalikian and Breslauer, 1996; Prehoda et al., 1998). So far, various experimental techniques have been developed to study the pressure-induced structural changes in proteins. Macroscopic compressibility determination via sound velocity measurement indicates that large internal compressibility exists inside proteins (Gekko and Noguchi, 1979; Gekko and Hasegawa, 1986). Microscopically, for example, fluorescence spectroscopy at high pressure detects structural changes by using the Trp residues as local probes (Weber and Drickamer, 1983); vibrational spectroscopy, like Raman and FTIR, is mainly used to detect the amide vibrational band that is conformation-sensitive (Takeda et al., 1995); in NMR spectroscopy, line-shape analysis (Wagner, 1980), paramagnetic chemical shifts (Morishima, 1987), coupling constant analysis (Urbauer et al., 1996) and so on have been used to detect local changes in structure and dynamics. Furthermore, the normal mode calculation (Yamato et al., 1993) and the molecular dynamics simulation (Kitchen et al., 1992; Wroblowski et al., 1996; Brunne and van Gunsteren, 1993) under high pressure are also performed to probe the protein behavior itself and the solvent effect on it. Only in one case, by applying x-ray crystallography, Kundrot and Richards (1987) detected a nonuniform compression in lysozyme at an atomic level. Many reviews about the pressure effect on protein structure are also available (Jonas and Jonas, 1994; Gross and Jaenicke, 1994; Heremans and Smeller, 1998).

As an alternative method to detect the structural changes at an atomic level under high pressure, we have recently developed an on-line high-pressure cell NMR system capable of recording spectra with high resolution at any pressure between 1 and 2000 bar (Akasaka et al., 1997, 1999; Li et al., 1998; Inoue et al., 1998). The essential part of this technique is to fit the high-pressure cell made of quartz inside the probe of the state-of-the-art NMR spectrometer (17.6T or 750 MHz for ^{1}H) without any modification of the probe (Yamada, 1974). Using this technique, we demonstrated in hen egg white lysozyme by one-dimensional ^{1}H measurement (Akasaka et al., 1997) that compaction occurs preferentially in the hydrophobic core, which shows consistent result with the x-ray crystallography study (Kundrot and Richards, 1987). In addition, by performing two-dimensional ^{1}H-NMR measurements at varying pressure between 1 and 2000 bar on bovine pancreatic trypsin inhibitor (BPTI), we discussed the origin of the pressure-induced chemical shift changes for individual amide protons (Li et al., 1998). The significant downfield shift tendency shown for almost all the amide protons suggested that individual

Received for publication 1 April 1999 and in final form 29 July 1999.

Address reprint requests to Dr. Kazuyuki Akasaka, Department of Molecular Science, Graduate School of Science and Technology, Kobe University, 1-1 Rokkodai-cho, Nada-ku, Kobe 657-8501, Japan. Tel.: +81-78-803-5687; Fax: +81-78-803-5688; E-mail: akasaka@kobe-u.ac.jp.

0006-3495/99/11/2801/12 $2.00

hydrogen bonds in BPTI are shortened under high pressure. Furthermore, by applying an empirical distance-shift relationship, intramolecular hydrogen bonds between amide protons and carbonyl oxygens were estimated to be shortened by ~1% at 2000 bar. Two other interesting aspects of the pressure-dependent amide proton shifts are found there. First, amides hydrogen-bonded to water have shifts larger than amides intramolecularly hydrogen-bonded, which implies that solvation layer between protein and water is more compressed. Second, significant variation in the magnitude of low field shifts exists among the amide groups involved in backbone-backbone hydrogen bonds, which implies that fluctuation is nonuniform in the hydrogen bond network. Similar phenomena were also observed in a small protein, gurmarin (Inoue et al., 1998).

More recently, the effect of pressure on amide ^{15}N chemical shifts was studied in uniformly ^{15}N-labeled BPTI in aqueous solution, by ^{1}H-^{15}N heteronuclear correlation spectroscopy between 1 and 2000 bar. Most ^{15}N signals were low field shifted linearly and reversibly, but nonuniformly, with pressure, suggesting a variation site-specific changes in ϕ, ψ angles in addition to decrease in distances between the amide nitrogen atom and its hydrogen-bond partner, the oxygen atom. So far, however, little has been studied of the pressure effect on the tertiary structure and dynamics in BPTI. In the present report, NMR observation is extended to practically all the protons of BPTI including C$^{\alpha}$ protons and side chain protons to focus on the tertiary structure changes induced by pressure. Here, not only pressure-induced chemical shifts but also pressure-induced changes in resonance line shape and nuclear Overhauser effect (NOE) were studied.

BPTI is chosen in this study because it is among the best-characterized and thoroughly studied proteins. Although it is a small protein with only 58 residues, it shows the essential feature of a globular protein. It has three S–S bonds, two antiparallel β-sheets, and two helices, as determined both by x-ray crystallography (Deisenhofer and Steigemann, 1975; Wlodawer et al., 1984, 1987; Parkin et al., 1995) and solution NMR spectroscopy (Wagner et al., 1987; Berndt et al., 1992). It is the protein to which high-pressure NMR was applied to find the pressure effects on the flip-flop motion of aromatic ring residues (Wagner, 1980). Its hydrogen exchange behavior was examined by FTIR under pressure (Goossens et al., 1996; Takeda et al., 1998). In addition, taking BPTI as an example, molecular dynamics simulation was also performed under high pressure (Wroblowski et al., 1996; Kitchen et al., 1992; Brunne and van Gunsteren, 1993).

MATERIALS AND METHODS

Sample preparation

Bovine pancreatic trypsin inhibitor (BPTI) was purchased from the Sigma Chemical Co. (St. Louis, MO) and was used without further purification. Crystals of BPTI were dissolved into 90% H_2O/10% D_2O containing 200 mM acetate-d_3 (Isotec Inc., Miamisburg, OH) buffer to make a 10 mM, pH 4.6 solution for NMR measurements.

High-pressure NMR apparatus

The high-resolution, high-pressure NMR technique employed here is a modification of the on-line high-pressure glass tube method originally reported by Yamada (1974). The protein solution is contained in a quartz tube (inner diameter of 1 mm, outer diameter of 3 mm, protected by a Teflon jacket), which is separated from the pressure mediator (kerosene) by a frictionless piston (Teflon) in a separator cylinder (BeCu). The pressure can be regulated at will between 1 and 2000 bar (measured with a Heise Bourdon gauge) with a hand pump remotely located from the 17.6T magnet (Japan Magnet Technology, Kobe, Japan), and is transmitted through a 6-m-long stainless steel tube containing kerosene to the sample solution in the NMR probe. A standard 5-mm ^{1}H selective NMR probe (Bruker) was used.

NMR spectroscopy

NMR spectra at varying pressures were measured on a Bruker DMX-750 spectrometer operating at a ^{1}H frequency of 750.13 MHz. The NOESY (Jeener et al., 1979; Macura et al., 1981) and TOCSY (Braunschweiler and Ernst, 1983) spectra at 36°C, and the TOCSY spectra at 57°C at various pressures were all obtained with spectral windows of 10 kHz with 256 complex points in the t_1 domain and 1024 complex points in the t_2 domain, using TPPI (Marion and Wuthrich, 1983) for phase-sensitive detection in the t_1 domain. Water suppression was accomplished by presaturation during the relaxation delay at high pressure or by using the pulsed-field gradient (PFG) WATERGATE (Piotto et al., 1992) technique incorporation of the 3-9-19 pulse sequence (Sklenar et al., 1993) at 1 bar. Chemical shifts were measured from the methyl signal of 3-(trimethylsilyl)[3,3,2,2-^{2}H] propionate-d_4 (TSP) at 0 ppm or from dioxane at 3.75 ppm, both added as internal references. The separation of the two signals was invariant with pressure within experimental error. A separate experiment showed that chemical shifts due to pH change [expected to be ~−0.3 pH unit at 2000 bar for the acetate buffer (Isaacs, 1981)] of the solution were negligibly small. Data were processed with the UXNMR package (Bruker) running on a Silicon Graphics Indigo2 workstation. The time domain data were zero-filled to 2048 and 1024 complex points in the t_1 and t_2 domains, respectively, and apodized using a quadratic sine-bell window function in both dimensions.

For the diffusion measurement, a slightly modified version of the spin echo experiment described by Altieri et al. (1995) was used. The standard Bruker PFG facility was used. No precise calibration of the gradient strength was performed, since we were interested only in the relative changes in the self-diffusion rates under pressure. Two sets of 14 one-dimensional experiments were recorded at 36°C at 30 and 2000 bar, respectively, with the strength of the encoding/decoding pulse field gradients being varied up to ~37.5 Gauss/cm. The NMR signal intensity, I, normalized to the signal intensity in the absence of gradient pulses, is related to the diffusion coefficient, D, by

$$I = \exp[-\gamma^2 g^2 \delta^2 D(\Delta - \delta/3)] \tag{1}$$

where γ is the gyromagnetic ratio of the observed nucleus; g and δ are the magnitude and duration of the magnetic field-gradient pulses, respectively, and Δ is the time between the gradient pulses. The experiments were performed with $\delta = 2$ ms, $g = 1$–37.5 G/cm, and $\Delta = 100$ ms at different pressures. Self-diffusion rates were obtained by using three-parameter exponential fitting of the signal intensity of methyl protons, I, against the square of the gradient strength, g^2. A computer simulation of line shape for a flip-flop exchange of an aromatic ring was performed with a home-made program on Macintosh.

RESULTS AND DISCUSSION

Pressure-induced chemical shifts of C^{α} protons and side chain protons

High-quality two-dimensional ^{1}H-NMR NOESY and TOCSY spectra were obtained on BPTI in 90% H_2O/10% D_2O, 200 mM acetate buffer at pH 4.6 and 36°C at various pressures between 1 and 2000 bar. ^{1}H chemical shift assignments at 1 bar were carried out according to the literature (Wagner et al., 1987; Berndt et al., 1992). Assignments at other higher pressures were obtained by comparing and closely correlating the crosspeaks in the NOESY and TOCSY spectra at 1 bar and those at the corresponding higher pressures. Practically most of the ^{1}H chemical shifts were analyzed at various pressures and they showed good linearity and reversibility within the pressure range from 1 to 2000 bar. Therefore, only the differences in chemical shift between 2000 bar and 1 bar are given in Table 1.

Histograms for the pressure-induced chemical shift changes [$\Delta\delta p = \delta(2000\text{ bar}) - \delta(1\text{ bar})$] for the C^{α} protons and side chain protons are shown in Fig. 1. The residues with odd numbers in sequence are shown in the solid column and those with even numbers are shown in the dotted column. The structural origin of pressure-induced strong downfield shifts for amide protons was carefully discussed in a previous paper (Li et al., 1998). In contrast to the amide protons, the C^{α} protons show sequence-dependent upfield and downfield pressure-induced shifts. In general, chemical shifts for the C^{α} protons are considered to be influenced mostly by the local external fields due to aromatic ring-currents and magnetic anisotropy effects from nearby peptide groups (Williamson and Asakura, 1993; Sitkoff and Case, 1998). It is known that the π-electrons of aromatic residues generate ring-currents around themselves that will constitute another shielding factor against the external field to the residues located close to them. The sign of ring-current shift is determined by the location and orientation of the affected proton and it can be either negative or positive. The magnitude of ring-current shift is a function of the distance between the affected proton and the corresponding aromatic residue that is proportional to r^{-3}, that is, the closer the distance, the stronger the ring-current shift that the C^{α} proton will receive. Ring-current shift is also one of the main reasons to cause chemical shift dispersion for ^{1}H-NMR signals of proteins in their folded states. Fig. 2 shows the ring-current shifts of C^{α} protons at 1 bar (*solid line*) calculated based on crystal structure at 1 bar using the program MOLMOL (Koradi et al., 1996), together with the pressure-induced chemical shifts (*dotted line*). It should be noted that the magnitude of the pressure-induced chemical shifts is magnified five times in Fig. 2. At atmospheric pressure, it is shown in Fig. 2 that the C^{α} protons of Cys-51, Pro-9, Ala-48, Gly-37, Arg-42, and Gly-12 receive strong negative ring-current shift effects from the aromatic residues of Phe-45, Phe-33, Tyr-21, Tyr-35, Phe-4, and Tyr-10, respectively; while those of Cys-5, Thr-11, Arg-20, Ala-40, Asn-43, and Asn-44 receive strong positive ring-current shift effects from Phe-4, Tyr-10, Phe-33, Tyr-10, Phe-45, and Phe-45, respectively. When pressure is applied to the system, strong upfield shifts are observed for the C^{α} protons of Cys-51, Pro-9, and Arg-42, and downfield shifts are observed for those of Arg-20, Arg-39, Ala-40, Asn-43, Asn-44, and Thr-54. Intriguingly, by comparing the pressure-induced shifts for C^{α} protons and the corresponding ring-current shifts at 1 bar, good consistency (not only the magnitude, but also the sign) is found for the residues of Cys-51, Pro-9, Arg-42 and Arg-20, Arg-39, Ala-40, Asn-43, and Asn-44.

According to the property of the ring-current shift described above, the C^{α} protons in which consistency was found would receive even stronger ring-current shifts caused by their adjacent aromatic residues due to distance shortening or compaction at high pressure. A similar trend was found for the first time for side chain protons in the high-pressure study on hen egg white lysozyme (Akasaka et al., 1997). Ring-current shifted signals observed in lysozyme indicated that a compaction occurs preferentially in the hydrophobic core of the protein. However, inconsistency also exists for the C^{α} protons of the residues like Cys-5, Thr-11, Gly-12, Ala-48, and Gly-37. This may suggest either that the ring-current shift is not the only reason to affect the chemical shifts of C^{α} protons under high pressure, or that in these regions, pressure causes the rings to go far away from the affected C^{α} protons.

Pressure-induced shifts for side chain protons are also shown as histograms in Fig. 1. Upfield shift tendency is obviously seen for most of the side chain protons. The average values of the pressure-induced shifts at 2000 bar for C^{β}, C^{γ}, C^{δ} (aliphatic), C^{δ} (aromatic), C^{ϵ} (aliphatic), C^{ϵ} (aromatic), and C^{ξ} (aromatic) protons are -0.013 ppm, -0.018 ppm, -0.025 ppm, -0.021 ppm, -0.042 ppm, 0.005 ppm, and -0.025 ppm, respectively. The average pressure-induced shifts for C^{α} protons is -0.014 ppm. It is interesting to note that pressure-induced shifts for C^{α} and C^{β} protons are close to each other on average, and are much smaller compared with other types of side chain protons. According to the magnitude of the average pressure-induced shifts, the side chain protons can be written in the increasing order C^{β}H, C^{γ}H, C^{δ}H, and C^{ϵ}H. A clear tendency is shown especially for the aliphatic side chain protons that the further they separate from the main chain, the larger pressure-induced shift they possess. This tendency may imply that the volume fluctuation is, in general, larger in the interior of the protein, namely that the side chain region is more flexible than the main chain part. The extremely small shift value for the aromatic C^{ϵ}H (0.005 ppm) results from slowed flip-flop motion, which will be discussed later in detail. In addition, it is interesting to find that, among all the detected side chain proton signals, extremely large upfield shifts are found specifically for βH of Arg-42 and Cys-51, δH of Pro-9 and Phe-45, and ϵH proton of Phe-45. If we recall ring-current shifts for C^{α} protons at 1 bar in Fig. 2, then we can find that the C^{α} protons of Arg-42 and Cys-51 give

TABLE 1 Chemical shift differences in 10 mM BPTI, pH 4.6, 36°C, 2 kbar–1 bar, 200 mM CD_3COOH buffer

Residue	NH	$C^{\alpha}H$	$C^{\beta}H$	$C^{\gamma}H$	$C^{\delta}H$	$C^{\varepsilon}H$	$C^{\xi}H$
Arg-1			0.003, −0.036	–, −0.055	−0.033, −0.074	−0.069	
Pro-2		0.010	–	–	−0.027, −0.001		
Asp-3	0.132	−0.028	−0.015, −0.015				
Phe-4	0.279	−0.008	−0.049, 0.037		−0.030, −0.030	−0.009, −0.009	0.002
Cys-5	−0.002	−0.053	−0.059. −0.021				
Leu-6	0.062	0.019	−0.004	0.010	0.001, −0.029		
Glu-7	0.022	0.013	–	–			
Pro-8		−0.035	−0.006, −0.033	−0.018, −0.018			
Pro-9		−0.083	−0.041, −0.005	−0.020, −0.028	−0.044, −0.096		
Tyr-10	0.109	−0.003	−0.011, −0.011		−0.014, −0.014	0.003, 0.003	
Thr-11	0.185	−0.029	0.001	−0.006			
Gly-12	0.152	−0.022, −0.009					
Pro-13		−0.002	−0.024, −0.003	−0.040	−0.021, −0.029		
Cys-14	0.084	0.034	−0.007, −0.053				
Lys-15	0.031	−0.010	−0.032, 0.012	−0.020			
Ala-16	0.003	−0.025	−0.014				
Arg-17	0.145	−0.042	0.007	−0.014	−0.014	−0.055	
Ile-18	0.073	−0.050	−0.027	−0.031, −0.028	−0.015		
Ile-19	0.145	−0.028	−0.006	0.038	−0.019		
Arg-20	0.044	0.033	−0.008	0.076, −0.139	−0.048, −0.011	0.021	
Tyr-21	0.105	−0.043	−0.059		−0.039, −0.039	0.011, 0.011	
Phe-22	−0.013	−0.060	0.022, 0.120		−0.005, −0.005	0.009, 0.009	−0.012
Tyr-23	0.098	−0.028	−0.005, 0.063		−0.039, −0.039	−0.035, −0.035	
Asn-24	−0.004	−0.015	−0.049, −0.026		−0.020, −0.003		
Ala-25	0.147	−0.027	−0.020				
Lys-26	0.178	−0.015	−0.007	−0.012			
Ala-27	0.115	−0.041	−0.004				
Gly-28	0.057	0.001, 0.016					
Leu-29	0.105	−0.001	0.058, 0.042				
Cys-30	0.040	0.037	0.020, −0.040				
Gln-31	0.035	−0.008	−0.019	−0.007			
Thr-32	0.098	−0.054	0.006	−0.021			
Phe-33	0.052	0.013	0.030		−0.021, −0.021	−0.013, −0.013	−0.033
Val-34	0.158	−0.019	−0.006				
Tyr-35	0.054	−0.061	0.011, −0.020		0.020, −0.022	0.017, −0.028	
Gly-36	0.153	−0.008, −0.026					
Gly-37	–	−0.052, 0.051					
Cys-38	0.000	−0.024	0.032, −0.033				
Arg-39	−0.019	0.051	−0.029	−0.032	−0.001	−0.028	
Ala-40	−0.008	0.039	−0.025				
Lys-41	0.104	−0.030	−0.035				
Arg-42	0.067	−0.069	−0.169, −0.212	−0.036, −0.041	−0.052, 0.005	−0.086	
Asn-43	0.053	0.039			−0.050, 0.002		
Asn-44	0.115	0.042	−0.007, −0.001				
Phe-45	0.015	−0.006	−0.017, −0.032		0.045, −0.089	0.357, −0.202	−0.058
Lys-46	−0.016	−0.008	−0.007, 0.005	−0.031			
Ser-47	0.009	−0.035	−0.017, −0.014				
Ala-48	0.003	−0.025	0.004				
Glu-49	0.005	0.025	−0.033, 0.000	−0.025, 0.014			
Asp-50	0.081	−0.030	0.021, 0.005				
Cys-51	0.046	−0.168	−0.060, −0.115				
Met-52	0.057	0.024		−0.018			
Arg-53	−0.022	−0.001	−0.010		0.008	−0.035	
Thr-54	−0.008	0.039	−0.006	0.020			
Cys-55	0.198	0.016	0.058, 0.045				
Gly-56	0.167	−0.023, −0.023					
Gly-57	0.112	−0.016, 0.009					
Ala-58	0.121	−0.035	−0.003				

–, Unassigned due to signal overlap.

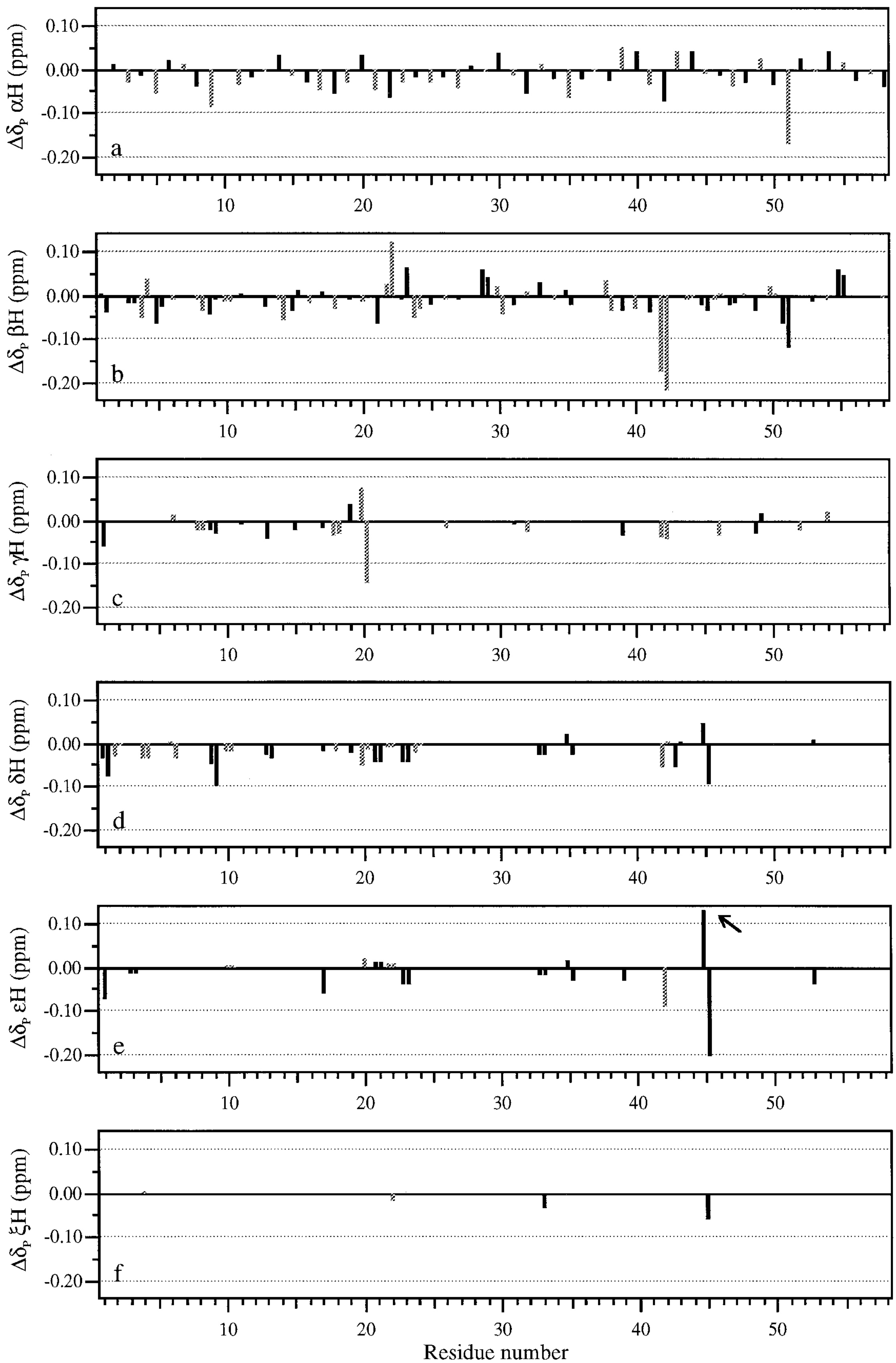

FIGURE 1 Histograms of the pressure-induced chemical shifts [$\Delta\delta p = \delta$(2000 bar) $-$ δ(1 bar)] for the C^{α} protons and side chain protons in the same scale. (*a*) αHs, (*b*) βHs, (*c*) γHs, (*d*) δHs, (*e*) ϵHs, and (*f*) ξHs. The amino acid residues with odd numbers are indicated in the solid column and those with even numbers are indicated in the dotted column. The arrow in (*e*) indicates that the pressure-induced shift of the ϵH of Phe-45 exceeds the scale required.

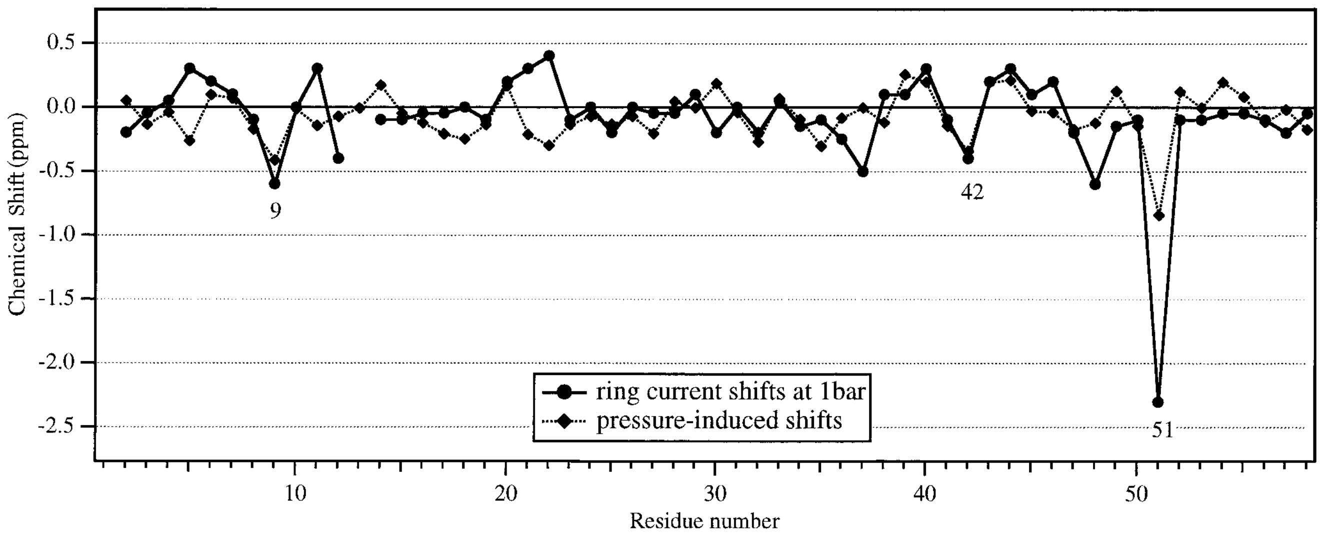

FIGURE 2 Plots of the pressure-induced shifts for C^{α} protons [$\Delta\delta p = \delta(2000\ \mathrm{bar}) - \delta(1\ \mathrm{bar})$] (○, ♦, *dotted line*; values magnified five times) and their ring-current shifts at 1 bar (♦, ●, *solid line*).

extremely large negative ring-current shift values. It is considered that the ring-current is also the main reason to cause upfield shifts of these protons. The large upfield shifts under pressure seemed to reflect the distance shortening between the βHs and their adjacent aromatic residues. Furthermore, the nonuniform upfield shift tendency for side chain protons would imply that site-specific compaction occurs inside the molecule at high pressure. Further details will be discussed later together with NOE data.

Pressure-induced changes in nuclear Overhauser effect

Direct evidence for the compaction of the tertiary structure was obtained from pressure-induced NOE changes. The intensity of NOE is related to the distance r between two different nuclear spins and the correlation time τ_c by an equation of the general form:

$$\mathrm{NOE}\ \alpha\ \mathrm{r}^{-6}\tau_c. \tag{2}$$

This would suggest that if we can assess τ_c independently, we will be able to obtain distance information through NOE measurements.

It is well known that the correlation time, τ_c, is related to the viscosity, η, in the following way:

$$\tau_c = 4\pi\eta a^3/3k_B T \tag{3}$$

where η is the viscosity, a is the dynamic radius of the protein, k_B is the Boltzmann constant, and T is the absolute temperature. At the same time, the viscosity, η, is related to the translational diffusion coefficient, D, in the following way:

$$D = k_B T/6\pi\eta a \tag{4}$$

where D is the diffusion coefficient of the solute, k_B, T, η, and a represent the same quantities as described in Eq. 3. Therefore, based upon the above consideration, we performed self-diffusion measurements by NMR at different pressures in order to finally obtain the pressure-dependent information of τ_c. The diffusion measurement and the related data processing are described in Materials and Methods. The result showed that the ratio of the self-diffusion coefficients measured at 2000 bar and 1 bar was 0.872. If we neglect the effect of pressure on the hydrodynamic nature of the protein, for example, its hydrodynamic radius, the decrease of self-diffusion coefficients would be considered to be due to the increase of solution viscosity, η, hence the increase of the correlation time, τ_c. According to the Eqs. 3 and 4, τ_c at 2000 bar is calculated to be increased by ~15% compared with the value at atmospheric pressure. Therefore, generally speaking, NOE intensities will be increased by the same amount as τ_c increases. In order to obtain pure distance information from NOE intensities, we calibrated the NOE intensities at 2000 bar to get rid of the pressure effect on τ_c. In addition, we take the diagonal peak of TSP as an intensity standard to compare NOE changes at different pressures, because the TSP peak is well separated with other peaks along the diagonal and it is assumed that pressure has no effect on its intensity.

As a typical and clear example, in Fig. 3 parts of the aromatic-aliphatic regions of the NOESY spectra are given to show the NOE changes at different pressures. All of the crosspeaks in Fig. 3 are assigned. It can be clearly seen that the NOE intensities between the βH of Arg-42 and the ring protons of Phe-4, i.e., δH and ϵH, were increased dramatically with pressure. Therefore, in this way, we obtained a list of pressure-induced NOE changes concerning the aromatic residues shown in Table 2, together with the chemical shift assignments. The list of the pressure-induced NOE

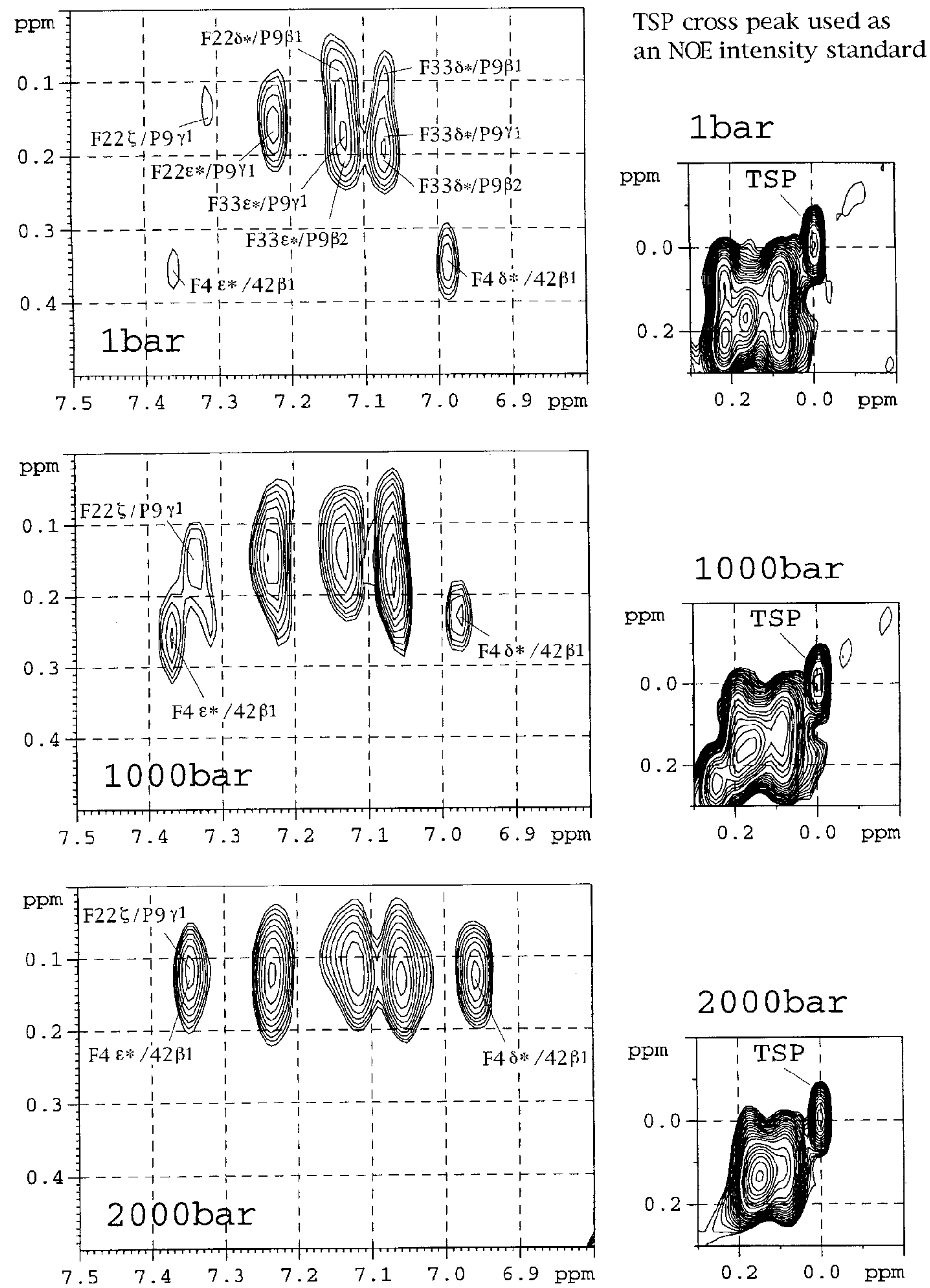

FIGURE 3 Parts of the aromatic-aliphatic regions of the NOESY spectra of BPTI, measured at 36°C and at 1 bar, 1000 bar, and 2000 bar with a mixing time of 150 ms. Assignments for all the crosspeaks are given. The diagonal peaks of TSP at different pressures, used as intensity standard, are also given.

changes of all other kinds of protons will be presented elsewhere. In Table 2, pressure-induced NOE changes are listed and categorized into two groups, namely, pressure-induced increased NOEs, which indicate compaction, are indicated by "+"; pressure-induced almost no change in NOEs by "±." Constraint pairs of Tyr-35δ_1H/Ile-18δH*, Phe-45ξH/Asn-43αH, Phe-45ξH/Thr-54γH*, and Phe-45HN/Arg-20β_1H demonstrate the compaction around Tyr-35 and Phe-45 from the NOE point of view. As shown in Table 2, compaction also occurs around Phe-4, Phe-22, and Tyr-23. NOE constraints for other aromatic residues like Tyr-10, Tyr-21, and Phe-33 have not been detected because of overlapping in spectra. To the authors' knowledge, this is the first instance that pressure-induced compaction is detected as NOE changes in the native manifold of proteins. Interestingly, if we recall the pressure-induced shifts shown in Fig. 1, we can find that the upfield shift of the βH of Arg-42 corresponds very well with its intensified NOE between ring protons of Phe-4.

Slowing of flip-flop motions by pressure

Flip-flop motion refers to the rotational motion of an aromatic ring around its Cβ and Cγ axis. For amino acid residues located in the interior of globular proteins, the

TABLE 2 The chemical shift assignments and pressure-induced NOE lists for the aromatic residues of BPTI at 57°C

Residue		Chemical shifts of aromatic ring protons at different pressures (ppm)						
		1 bar	500 bar	1000 bar	1500 bar	2000 bar	NOE constraints[#]	Pressure-induced NOE changes[§]
Phe-4	$C^{\delta}H$ (2, 6H)	7.00	6.99	6.98	6.98	6.98	Phe-4δH*/Arg-42β_2H	+
	$C^{\epsilon}H$ (3, 5H)	7.37	7.37	7.37	7.37	7.37	Phe-4εH*/Arg-42β_2H	+
	$C^{\zeta}H$ (4H)	7.32	7.32	7.32	7.32	7.33		
Tyr-10	$C^{\delta}H$ (2, 6H)	7.33	7.33	7.33	7.33	7.33		
	$C^{\epsilon}H$ (3, 5H)	7.08	7.09	7.09	7.09	7.09		
Tyr-21	$C^{\delta}H$ (2, 6H)	6.80	6.80	6.80	6.80	6.82		
	$C^{\epsilon}H$ (3, 5H)	6.72	6.72	6.70	6.68	6.68		
Phe-22	$C^{\delta}H$ (2, 6H)	7.15	7.14	7.15	7.14	7.15	Phe-22εH*/Pro-9γ_1H	+
	$C^{\epsilon}H$ (3, 5H)	7.22	7.23	7.22	7.23	7.23		
	$C^{\xi}H$ (4H)	7.26	7.27	7.27	7.26	7.26		
Tyr-23	$C^{\delta}H$ (2, 6H)	7.19	7.17	7.17	7.16	7.16	Tyr-23εH*/Ala-25βH*	+
	$C^{\epsilon}H$ (3, 5H)	6.34	6.34	6.33	6.32	6.32	Thr-23εH*/Cys-5β_1H	±
Phe-33	$C^{\delta}H$ (2, 6H)	7.07	7.07	7.06	7.07	7.07		
	$C^{\epsilon}H$ (3, 5H)	7.13	7.12	7.12	7.12	7.12		
	$C^{\xi}H$ (4H)	7.00	6.99	6.98	6.98	6.98		
Tyr-35	$C^{\delta}H$ (2, 6H)	7.76, 6.69	7.76, 6.68	7.77, 6.67	7.78, 6.68	7.78, 6.68	Tyr-35δ_1H/Ile-18δH*	+
	$C^{\epsilon}H$ (3, 5H)	6.82	6.78, 6.83	6.77, 6.86	6.77, 6.87	6.77, 6.88	Tyr-35HN/Ile-19βH*	±
							Tyr-35HN/Ile-19γH*	±
Phe-45	$C^{\delta}H$ (2, 6H)	7.38	7.38	7.38	7.38	7.38	Phe-45HN/Arg-20β_1H	+
	$C^{\epsilon}H$ (3, 5H)	7.88	7.89	—[¶]	—[¶]	—[¶]	Phe-45ξH/Asn-43αH	+
	$C^{\xi}H$ (4H)	7.62	7.63	7.65	7.66	7.66	Phe-45ξH/Thr-54γH*	+
							Phe-45ξH/Thr-54βH	±

[#]The amino acid residue is identified by a three-letter symbol, followed by a number indicating the position in the amino acid sequence. The superscript asterisk indicates pseudoatoms that substitute for a group of two or more protons. The subscript number followed by Greek letters indicates the exact proton with the same kind, in which "1" and "2" are defined according to the size of chemical shift in assignments at 1 bar instead of stereo assignment.
[§]Pressure-induced NOE changes are indicted by two symbols, in which "+" stands for increased NOE and "±" for no NOE change.
[¶]Chemical shift unassignable due to lineshape broadening.

influence of the environment can lead to quite sizable chemical shifts. For the aromatic rings of phenylalanine and tyrosine, the covalent structure is symmetrical with respect to a twofold axis through the Cβ-Cγ bond. Provided that all the aromatic protons experience the same environment, this symmetry is manifested in the equivalence of the chemical shifts of the 2,6- and 3,5-protons. In globular proteins, however, the environment of the aromatic rings is characterized by a nonperiodic distribution of structural elements. As a consequence, individual ring protons may experience different microenvironments and hence show different chemical shifts (Wüthrich, 1986). When the aromatic rings undergo rapid rotational motions about the Cβ-Cγ bond, a symmetrical spectrum is again obtained. Therefore, flip-flop motion reflects the dynamic feature of a protein.

In the present report, two-dimensional $^1H/^1H$ TOCSY spectra were measured at 57°C at varying pressure. The aromatic-aromatic regions measured at 57°C at different pressures with an interval of 500 bar are shown in Fig. 4 *A*. The resolution of the spectra is greatly improved with the help of the two-dimensional NMR technique. The assignments are given for the crosspeaks of all the aromatic residues in BPTI, as was shown in Table 2. It is clearly seen that, with increasing pressure, the crosspeaks for residues Phe-4, Tyr-10, Tyr-21, Phe-22, Tyr-23, and Phe-33 show almost no changes in chemical shift and line shape. However, those for Tyr-35 and Phe-45 show great changes in both chemical shift and line shape. As for Phe-45, five aromatic protons, i.e., 2H, 6H, 4H, 3H, and 5H, constitute a spin system of AA′MXX′. At atmospheric pressure, the intensities of the crosspeaks between 2, 6H and 4H, and between 3, 5H and 4H, and between 3, 5H and 2, 6H are strong (Fig. 4 *A*, *top*). The signals of 2H and 6H are found at identical chemical shifts (7.38 ppm) and those of 3H and 5H at 7.88 ppm, showing that the flip-flop motion of the Phe-45 ring is rapid enough to average out the chemical shifts between 2H and 6H and between 3H and 5H. At higher pressures, the intensities of these crosspeaks become weaker, suggesting that the signals are broadened out presumably due to slowing of the flip-flop motion of Phe-45.

For Tyr-35, four aromatic protons, i.e., 2H, 6H, 3H, and 5H, constitute a spin system of AA′BB′. The process of the spectral change with pressure can be seen more clearly in the one-dimensional slice spectra shown in Fig. 4 *B*. Here, slices are taken at the chemical shift position of 2H of Tyr-35 along the horizontal direction (↔). At the atmospheric pressure, 2H and 6H give separate chemical shifts at 7.76 ppm and 6.69 ppm, while the signals of 3H and 5H merge into a singlet at 6.82 ppm. With increasing pressure, the 6H signal becomes sharper, and the merged signals of 3H and 5H become separated as two sharp signals at 6.77 ppm and 6.88 ppm, respectively. These spectral changes qualitatively indicate that the flip-flop rate of the Tyr-35 ring is slowed down at high pressure.

For a quantitative estimation of the flip rates, spectral simulation was carried out for the slice (or cross-section)

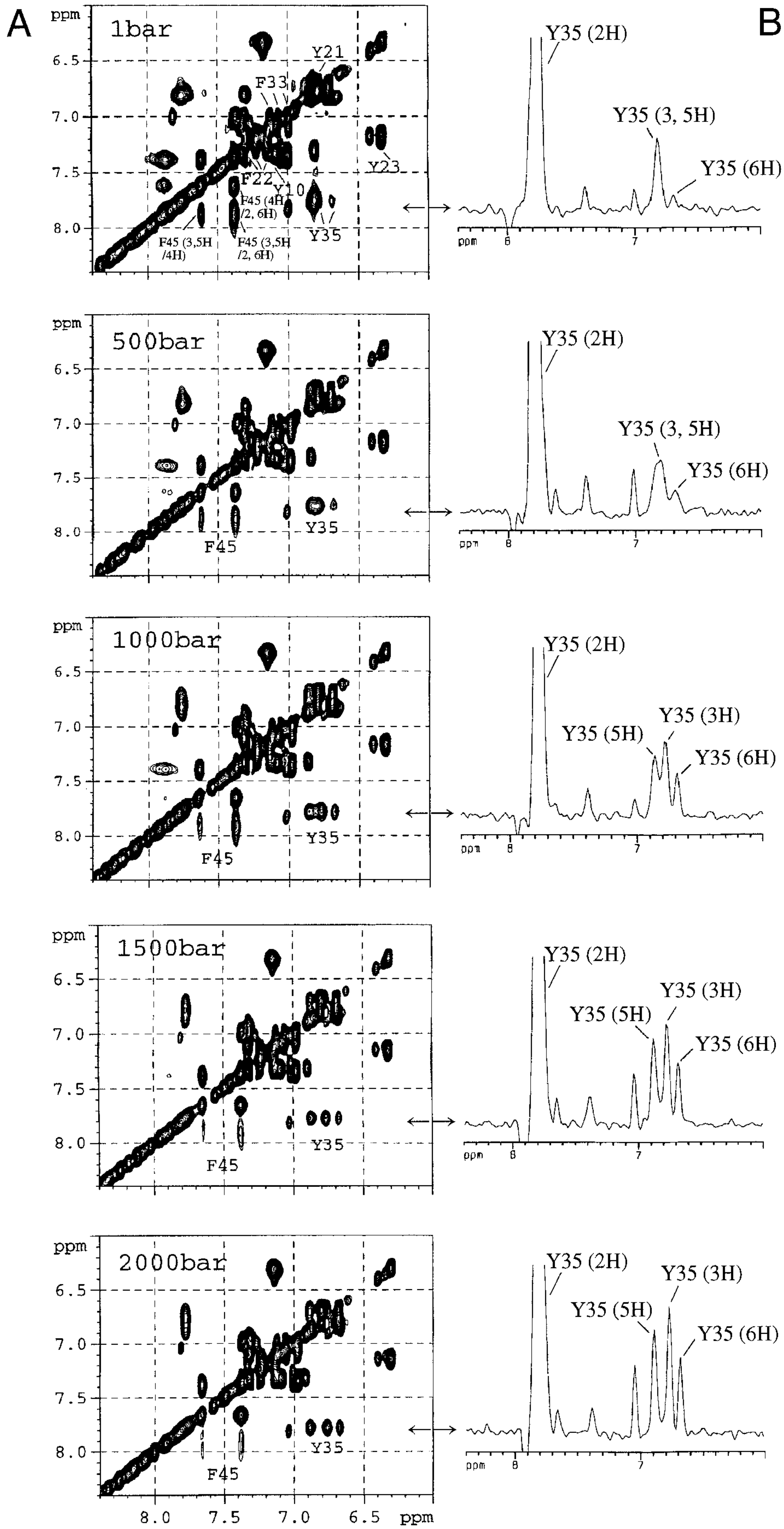

FIGURE 4 (*A*) Aromatic-aromatic regions of two-dimensional TOCSY spectra of BPTI at various pressures at 57°C. (*B*) Cross-sections (or slices) of the TOCSY spectra at the resonance position of 2H of Tyr-35.

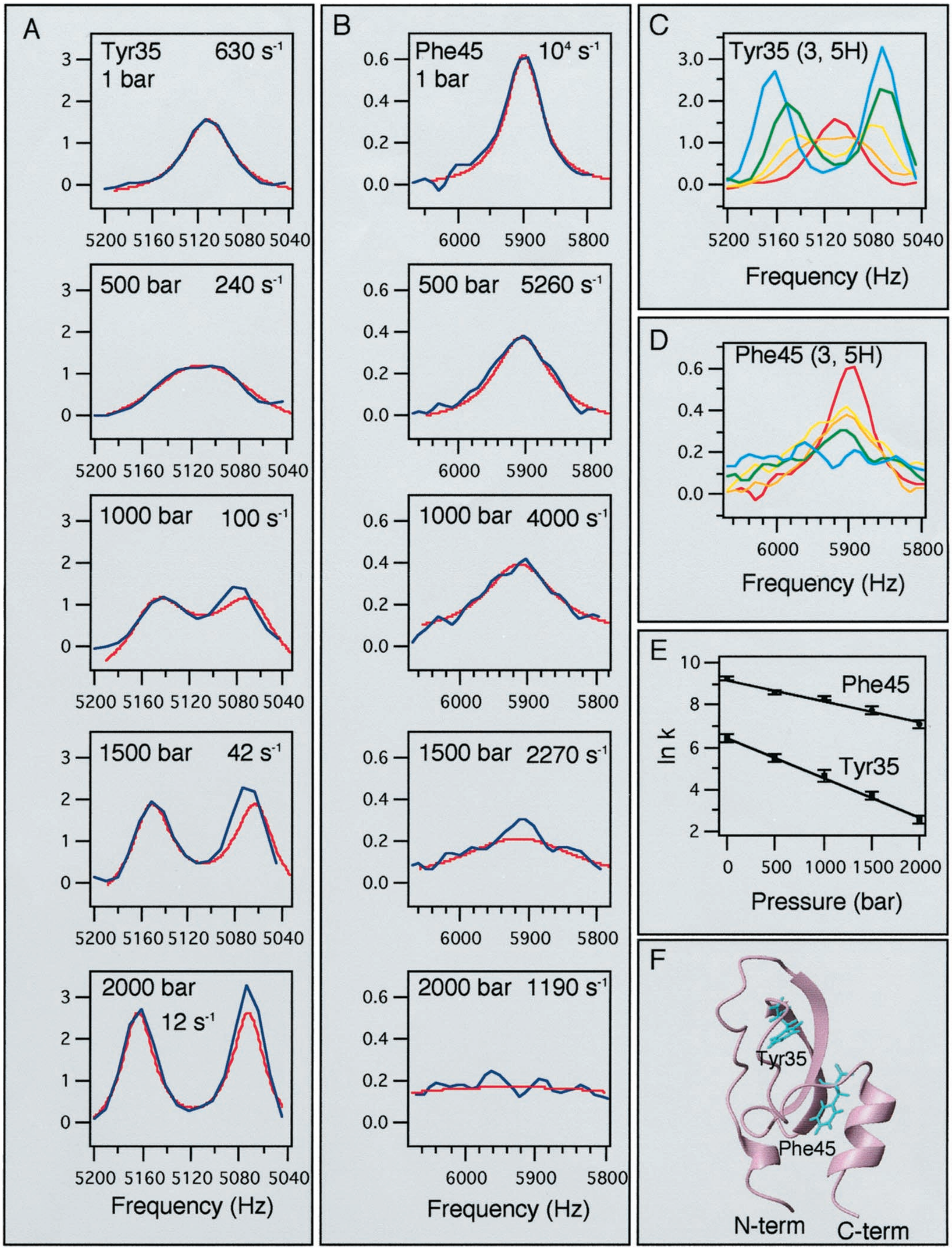

FIGURE 5 (*A*) Experimental (*blue*) and simulated (*red*) spectra of 3H and 5H of Tyr-35 at different pressures. (*B*) Experimental (*blue*) and simulated (*red*) spectra of 3H and 5H of Phe-45 at different pressures. In these simulations, it was assumed that the intrinsic chemical shifts of 3H and 5H of Tyr-35 are separated by 96 Hz, and those of 3H and 5H of Phe-45 by 486 Hz, while their intrinsic linewidths are 29 Hz, all of which were determined by separate measurements at low temperature. (*C*) Superposition of the 3H and 5H region of the TOCSY slice spectra taken at 2H resonance position of Tyr-35 measured at 57°C at five different pressures: 1 bar (*red*), 500 bar (*orange*), 1000 bar (*yellow*), 1500 bar (*green*), and 2000 bar (*cyan*). (*D*) Superposition of the 3H and 5H region of the TOCSY slice spectra taken at 2H resonance position of Phe-45 measured at 57°C at five different pressures: 1 bar (*red*), 500 bar (*orange*), 1000 bar (*yellow*), 1500 bar (*green*), and 2000 bar (*cyan*). (*E*) Logarithmic plot of the flip-flop rate of the ring, k (in s^{-1}), for Tyr-35 and Phe-45 against pressure. (*F*) A ribbon model for BPTI with locations of Tyr-35 and Phe-45.

spectra of the experimental two-dimensional TOCSY spectra for Tyr-35 and Phe-45. One cross-section was taken at the chemical shift position of 2H of Tyr-35 (7.76–7.78 ppm, indicated by arrows), and are shown in the right-hand side (Fig. 4 *B*). The other cross-section was taken at the chemical shift position of 4H of Phe-45 (~7.62 ppm). Out of these cross-sectional spectra, resonances of 3H and 5H of Tyr-35 and Phe-45 were chosen and are given superimposed for different pressures in Fig. 5, *C* and *D*. The exchange broadening and resonance coalescence of 3H and 5H signals are clear, showing pressure-induced reduction of the flip rate. The slightly uneven intensities for H5 and for H3 in Fig. 5 *C* at 1000, 1500, and 2000 bar are due to the overlap of the 6H signal of Tyr-35. At each pressure, simulation was performed, and the result for Tyr-35 is shown in Fig. 5 *A* as a series of superimposed experimental (*blue*) and simulated (*red*) spectra. In Fig. 5 *B*, the same for 3H and 5H of Phe-45 are shown. The flip-flop rates of both Tyr-35 and Phe-45 rings of BPTI, which span a relatively slow frequency range of 10^1-10^4 s^{-1} (or $\tau = 0.1$–100 ms), show significant retardation by a factor of 10^1-10^2 at 2000 bar.

In Fig. 5 *E*, logarithms of the flip rates obtained from the simulation are plotted against pressure. The slope of the plot gives the activation volume through the relation

$$\Delta V^{\ddagger} = -k_B T \left(\frac{\partial \ln k}{\partial P} \right)_T \quad (5)$$

where $\Delta V^{\ddagger}$ is the activation volume, k_B is the Boltzmann constant, T is the absolute temperature, and k is the flip rate. In Fig. 5 *E*, the plot can be fitted well with a straight line up to 2 kbar, giving pressure-independent activation volumes to be 85 ± 20 Å^3 (or 51.2 ml/mol) and 46 ± 9 Å^3 (or 27.7 ml/mol) for Tyr-35 and Phe-45, respectively. Namely, in the activated states the protein must expand by 46 and 85 Å^3 around the Tyr-35 and Phe-45 rings, respectively. The present analysis confirms the result of the earlier pioneering work on activation volumes of BPTI, i.e., 60 ± 20 Å^3 for Tyr-35 and 50 ± 10 Å^3 for Phe-45, using one-dimensional NMR in the pressure range up to ~1200 bar (Wagner, 1980).

The activation volume is defined as a difference between the volume occupied by the ring in the ground state and the volume in the activated state. If we assume that the volume in the activated state is the volume occupied by a rotating Tyr or Phe ring and is equal to 164 Å^3 with a radius of 3.4 Å (Wagner, 1980), the activation volumes (85 ± 20 Å^3 for Tyr-35 and 46 ± 9 Å^3 for Phe-45) give 79 Å^3 and 118 Å^3 for the volumes occupied by the Tyr-35 and Phe-45 rings, respectively, in the equilibrium conformation. While the small occupied volume (79 Å^3) by Tyr-35 means a close packing around the Tyr-35 ring, the large occupied volume (118 Å^3) by Phe-45 would probably correspond to a loose packing around the Phe-45 ring. This expectation is borne out partly by the fact that the flip is two orders of magnitude more frequent for Phe-45 than for Tyr-35. If, as the NOE increase suggests, the packing density increases around these aromatic residues, the activation volume should, in principle, be pressure-dependent. However, the straight line in Fig. 5 shows the effect of compaction on activation volumes is apparently small.

It would be interesting to compare these activation volumes with the equilibrium volume fluctuation of the protein. Although there is no direct measurement for BPTI, a reasonable estimate of the root-mean-squares fluctuation would be $0.3 \pm 0.1\%$ of the total volume of the protein (Gekko and Hasegawa, 1986), i.e., only ~24 Å^3. Thus the local volume fluctuation may far exceed the root-mean-squares fluctuation of the entire protein molecule. This result suggests that the formation of a large local cavity may be a consequence of accumulation of smaller cavities. The result appears to be consistent with the dynamic nature of cavity formation (Kocher et al., 1996) or a mobile defect model (Lumry and Rosenberg, 1975; Pain, 1987). The result is also an interesting example showing that critical fluctuations of a protein molecule, as manifested by ring-flips occurring in millisecond range, take place in a range far from the range of equilibrium fluctuation.

The pressure reduction of the flip rates may be compared with the reduction of the flip rate by lowering temperature (Wuthrich, 1986). By comparing line shapes, we notice that the reduction of the flip rates for Tyr-35 and Phe-45 by pressure at 2000 bar at 57°C is nearly equivalent to lowering temperature by ~25° to ~30–35°C at 1 bar.

CONCLUSIONS

Structural information obtained by using an on-line variable-pressure NMR technique provides useful insight into microscopic compressibility and volume fluctuation in proteins. Analysis of three kinds of NMR parameters, i.e., chemical shifts, NOE, and line shape, indicates that the main effect of high pressure is a specific compaction of the tertiary structure and a change in slow internal motions. Rates of the flip-flop motions of the Tyr and Phe rings are significantly retarded by pressure, showing large activation volumes. Overall, high-pressure NMR is a powerful tool to study microscopic compressibility and dynamics of a globular protein.

This work was supported by a grant-in-aid for Scientific Research from the Ministry of Education, Science, Sports and Culture of Japan.

REFERENCES

Akasaka, K., H. Li, H. Yamada, R. Li, T. Thoresen, and C. K. Woodward. 1999. Pressure response of protein backbone structure. Pressure-induced amide ^{15}N chemical shifts in BPTI. *Protein Sci.* 8, in press.

Akasaka, K., T. Tezuka, and H. Yamada. 1997. Pressure-induced changes in the folded structure of lysozyme. *J. Mol. Biol.* 271:671–678.

Altieri, A. S., D. P. Kinton, and R. A. Byrd. 1995. Association of biomolecular systems via pulsed field gradient NMR self-diffusion measurements. *J. Am. Chem. Soc.* 117:7566–7567.

Berndt, K. D., P. Guntert, L. P. M. Orbons, and K. Wuthrich. 1992. Determination of a high-quality nuclear magnetic resonance solution structure of the bovine pancreatic trypsin inhibitor and comparison with three crystal structures. *J. Mol. Biol.* 227:757–775.

Braunschweiler, L., and R. R. Ernst. 1983. Coherence transfer by isotropic mixing: application to proton correlation spectroscopy. *J. Magn. Reson.* 53:521–528.

Brunne, R. M., and W. F. van Gunsteren. 1993. Dynamical properties of bovine pancreatic trypsin inhibitor from a molecular dynamics simulation at 5000 atm. *FEBS Lett.* 323:215–217.

Chalikian, T. V., and K. J. Breslauer. 1996. On volume changes accompanying conformational transitions of biopolymers. *Biopolymers.* 39: 619–626.

Deisenhofer, J., and W. Steigemann. 1975. Crystallographic refinement of the structure of bovine pancreatic trypsin inhibitor at 1.5 Å resolution. *Acta Crystallogr. B.* 31:238–250.

Gekko, K., and Y. Hasegawa. 1986. Compressibility-structure relationship of globular proteins. *Biochemistry.* 25:6563–6571.

Gekko, K., and H. Noguchi. 1979. Compressibility of globular proteins in water at 25°C. *J. Phys. Chem.* 83:2706–2714.

Goossens, K., L. Smeller, J. Frank, and K. Heremans. 1996. Pressure-tuning the conformation of bovine pancreatic trypsin inhibitor studied by Fourier-transform infrared spectroscopy. *Eur. J. Biochem.* 236:254–262.

Gross, M., and R. Jaenicke. 1994. The influence of high hydrostatic pressure on structure, function and assembly of proteins and protein complexes. *Eur. J. Biochem.* 221:617–630.

Heremans, K., and L. Smeller. 1998. Protein structure and dynamics at high pressure. *Biochim. Biophys. Acta.* 1836:353–370.

Inoue, K., H. Yamada, T. Imoto, and K. Akasaka. 1998. High pressure NMR study of a small protein, gurmarin. *J. Biomol. NMR.* 12:535–541.

Isaacs, N. S. 1981. Liquid-Phase High-Pressure Chemistry, Chap. 3. John Wiley and Sons, New York.

Jeener, T., B. H. Meier, P. Bachmann, and R. R. Ernst. 1979. Investigation of exchange processes by two-dimensional NMR spectroscopy. *J. Chem. Phys.* 71:4546–4553.

Jonas, A., and J. Jonas. 1994. High-pressure NMR spectroscopy of proteins and membranes. *Annu. Rev. Biophys. Biomol. Struct.* 23:287–318.

Kitchen, D. B., L. H. Reed, and R. M. Levy. 1992. Molecular dynamics simulation of solvated protein at high pressure. *Biochemistry.* 31: 10083–10093.

Kocher, J. P., M. Prevost, S. J. Wodak, and B. Lee. 1996. Properties of the protein matrix revealed by the free energy of cavity formation. *Structure.* 4:1517–1529.

Koradi, R., M. Billeter, and K. Wuthrich. 1996. MOLMOL: a program for display and analysis for macromolecular structures. *J. Mol. Graph.* 14:51–55.

Kundrot, C. E., and F. M. Richards. 1987. Crystal structure of hen egg-white lysozyme at a hydrostatic pressure of 1000 atmospheres. *J. Mol. Biol.* 193:157–170.

Li, H., H. Yamada, and K. Akasaka. 1998. Effect of pressure on individual hydrogen bonds in proteins. Basic pancreatic trypsin inhibitor. *Biochemistry.* 37:1167–1173.

Lumry, R., and A. Rosenberg. 1975. The mobile defect hypothesis of protein function. *Coll. Int. CNRS L'Eau. Syst. Biol.* 246:55–63.

Macura, C., Y. Huang, D. Suter, and R. R. Ernst. 1981. Two-dimensional chemical exchange and cross-relaxation spectroscopy of coupled nuclear spins. *J. Magn. Reson.* 43:259–281.

Marion, D., and K. Wuthrich. 1983. Application of phase sensitive two-dimensional correlated spectroscopy (COSY) for measurements of H-1-H-1 spin-spin coupling-constants in proteins. *Biochem. Biophys. Res. Commun.* 113:967–974.

Morishima, I. 1987. Current Perspectives of High-Pressure Biology. Academic Press, New York. 315–333.

Pain, R. H. 1987. Protein structure. New light on old defects. *Nature.* 326:247.

Parkin, S., B. Rupp, and H. Hope. 1995. Protein Data Bank (1BPI). Brookhaven National Laboratory, Upton, NY.

Piotto, M., V. Saudek, and V. Sklenar. 1992. Gradient-tailored excitation for single-quantum NMR spectroscopy of aqueous solutions. *J. Biomol. NMR.* 2:661–665.

Prehoda, K. E., E. S. Mooberry, and J. L. Markley. 1998. Pressure denaturation of proteins: evaluation of compressibility effects. *Biochemistry.* 37:5785–5790.

Sitkoff, D., and D. A. Case. 1998. Theories of chemical shift anisotropies in proteins and nucleic acids. *Prog. Nucl. Magn. Reson. Spectrosc.* 32:165–190.

Sklenar, V., M. Piotto, R. Leppik, and V. Saudek. 1993. Gradient-tailored water suppression for H-1-N-15 HSQC experiments optimized to retain full sensitivity. *J. Magn. Reson., Ser. A.* 102:241–245.

Takeda, N., M. Kato, and Y. Taniguchi. 1995. Pressure- and thermally induced reversible changes in the secondary structure of ribonuclease A studied by FT-IR spectroscopy. *Biochemistry.* 34:5980–5987.

Takeda, N., K. Nakano, M. Kato, and M. Taniguch. 1998. Pressure-induced structural rearrangements of bovine pancreatic trypsin inhibitor studied by FTIR spectroscopy. *Biospectroscopy.* 4:209–216.

Urbauer, J. L., M. R. Ehrhardt, R. J. Bieber, P. F. Flynn, and A. J. Wand. 1996. High-resolution triple-resonance NMR spectroscopy of a novel calmodulin-peptide complex at kilobar pressure. *J. Am. Chem. Soc.* 118:11329–11330.

Wagner, G. 1980. Activation volumes for the rotational motion of interior aromatic rings in globular proteins determined by high resolution ^{1}H-NMR at variable pressure. *FEBS Lett.* 112:280–284.

Wagner, G., W. Braun, T. F. Havel, T. Schumann, N. Go, and K. Wüthrich. 1987. Protein structures in solution by nuclear magnetic resonance and distance geometry. The polypeptide fold of the basic pancreatic trypsin inhibitor determined using two different algorithms, DISGEO and DISMAN. *J. Mol. Biol.* 196:611–639.

Weber, G., and H. G. Drickamer. 1983. The effect of high pressure upon proteins and other biomolecules. *Q. Rev. Biophys.* 16:89–112.

Williamson, M. P., and T. Asakura. 1993. Empirical comparisons of models for chemical-shift calculation in proteins. *J. Magn. Reson., Ser. B.* 101:63–71.

Wlodawer, A., J. Nachman, G. L. Gilliland, W. Gallagher, and C. Woodward. 1987. Structure of form III crystals of bovine pancreatic trypsin inhibitor. *J. Mol. Biol.* 198:469–480.

Wlodawer, A., J. Walter, R. Huber, and L. Sjolin. 1984. Structure of bovine pancreatic trypsin inhibitor. Results of joint neutron and x-ray refinement of crystal form II. *J. Mol. Biol.* 193:145–156.

Wroblowski, B., J. F. Diaz, K. Heremans, and Y. Engelborghs. 1996. Molecular mechanisms of pressure induced conformational changes in BPTI. *Proteins: Struct., Funct., Genet.* 25:446–455.

Wüthrich, K. 1986. NMR of proteins and nucleic acids. John Wiley and Sons, New York.

Yamada, H. 1974. Pressure-resisting glass cell for high pressure, high resolution NMR measurement. *Rev. Sci. Instrum.* 45:640–642.

Yamato, T., J. Higo, Y. Seno, and N. Go. 1993. Conformational deformation in deoxymyoglobin in hydrostatic pressure. *Proteins: Struct., Funct., Genet.* 16:327–340.